Responses to CC2:

General comments:

Obtaining a high-resolution long-term precipitation oxygen isoscape dataset can be critical for relevant hydrological studies. This study presented a first attempt to solve this issue, really appreciate, but from my point of view, it is still a rather premature dataset and have limited value. The authors downscaled and fused eight iGCMs precipitation oxygen isoscape using five different methods from a coarse spatial resolution (~2/3 degree) to a higher spatial resolution (0.5 degree). However, the work is not innovative and no important and robust findings were obtained.

Re: We would like to thank the reviewer for the time taking in reviewing our manuscript and providing constructive comments. The crux of the paper is to develop a long-term high-spatiotemporal resolution dataset for the mainland of China using an optimal hybrid approach, which is the best of the existing datasets available so far in the country. Following these suggestions, we have carefully revised the manuscript, especially for the validation of the dataset's quality and presenting the robust findings. Below please find our point-by-point responses to these comments.

With the motivations of resolving the lack and uneven distribution of observations, as well as the coarse and biased iGCM simulations, this study takes a hybrid approach that makes full use of observations to integrate the advantages of various iGCMs by using the optimal combination of data fusion and bias correction methods. In other words, the devised approach used all observations and iGCM simulations to the utmost extent to ensure the highest accuracy possible throughout the entire time period. This is a first attempt to develop such a dataset in China, which is of great importance in providing a data foundation for the study of complex hydrological and climatic systems.

The fusion and bias correction methods in the study have been widely used; however, to the best of our knowledge they have not been used in the field of stable isotopes. This study first compared the performance of these methods to find the best combination to build the dataset for different time periods by regions. The results showed that the CNN fusion method consistently performed the best for all sub-regions in China, and two bias correction methods (LS and DT) showed similar performance. The combination of the CNN fusion and bias correction methods is satisfactory to develop a high-resolution isoscape with a long time period. In other words, in order to maximize the utilization of available data, the CNN fusion method was used for the common period of all climate simulation and observations, while the bias correction methods were used for the periods with only one or two climate simulations, and with no observations. Considering China is a large country with various climatic conditions and complex terrain, the selected methods may also be able to be applied to other regions of the world.

Definitely, we agree with the reviewer that the dataset quality is the primary concern, and the quality was not well evaluated in the original manuscript. In the revision of this manuscript, following the reviewers' specific comments, a comprehensive assessment of the dataset at a finer scale was conducted. Specifically, the dataset was evaluated with respect to reproducing the time-series of in-situ observations at station scale, as well as the spatial pattern for each month. The results show that the in-situ observations were reasonably represented by the isoscape time series for all stations. The correlation coefficients between the isoscape simulations and observations are larger than 0.8 for 73% of the stations and larger than 0.9 for 49% of the stations. The root mean square errors between the isoscape simulations and observations are smaller than 20‰ for 78% of the stations and less than 15‰ for 56% of the stations. From the monthly spatial distribution of isotopes, CNN fusion simulations also capture the spatial pattern of observations most accurately. All results

showed that the isoscape dataset is of high quality. **The detailed results can be found in the responses to specific comments below.**

The results do not convince me since this method highly depends on the training data, which cover a short period, are unevenly distributed across regions, and insufficient to train model.

Re: We also agree with the reviewer that the time period of observed data is short for some stations. However, the monthly data were used in our study. More importantly, to partly solve the problem of short period, the data fusion and bias correction were conducted at the regional scale for a specific season to pool multiple sub-datasets together for training the neural network models and bias correction methods. In other words, the training of model was not conducted for each individual station. Moreover, considering the lack of observed data for training, we chose the simple structure to make the network not too deep with desirable results. For example, we chose the 1D convolutional neural network because of its advantages for data scarcity (Kiranyaz et al., 2021). Moreover, we only used the convolutional neural networks (CNN) fusion method to generate the dataset for the 1969-2007 period, which is more dependent on training data. For this period, the observed and iGCM simulations are relatively abundant. In other periods, bias correction methods were used, which are relatively less dependent on observations. Moreover, from the refined dataset evaluation (detailed results can be seen in the last part), the in-situ observations were reasonably represented by the isoscape time series at station scale, and the spatial pattern was captured most accurately for each month. All results showed that the CNN fusion method performs well, and the established dataset is of high quality and reliable.

Definitely, the models might perform even better if more observations were available. But then again, the lack of observations is the main motivation to develop this dataset, as we were attempted to maximize the utilization of available data from all observations and climate model simulations. In addition, we will introduce some physical-based ancillary data in the fusion processes, such as elevation and meteorological data, to fine tune the data and make our dataset more reliable.

References:

Kiranyaz, S., Avci, O., Abdeljaber, O., Ince, T., Gabbouj, M., and Inman, D. J.: 1D convolutional neural networks and applications: A survey, Mechanical systems and signal processing, 151, 107398, https://doi.org/10.1016/j.ymssp.2020.107398, 2021.

Moreover, as we know, the precipitation oxygen isoscape is highly dependent on local climate conditions, terrain factors, as well as large-scale atmospheric and local circulation. No such physical-based ancillary data were used in this study, which limited the further applications of produced 0.5-degree data. The sub-pixel spatial patterns within a coarse pixel changes, but the current methodology cannot get this information.

Re: Thank you for your suggestions. We agree with the review that the local climatic conditions, terrain and other factors may need to be considered in data fusion. In the revised manuscript, we will introduce some physical-based ancillary data in the fusion, such as elevation and meteorological data, to enrich the information in the process of data fusion. These data are closely related to precipitation isotopes and are easily accessible.

The considered ancillary data include Shuttle Radar Topography Mission digital elevation data (SRTM DEM) with the spatial resolution of 90m, and dataset of gridded monthly precipitation and temperature in China with spatial resolution of the 0.5 degree.

The generation of isoscape taking into account ancillary data can be divided into five steps. (1) Prior to generating the dataset, inverse distance weighting (IDW) method was used to interpolate all iGCM simulations and ancillary data to observation stations. (2) Three neural network data fusion and two bias correction methods were trained using observations and iGCM simulations for all months within a season and all stations within a sub-region. For the fusion methods, ancillary data were also included in the training process. (3) The performance of each model was evaluated for the validation period by the cross-validation method to find the optimal data fusion and bias correction methods. (4) All iGCM simulations and ancillary data were interpolated to the LMDZ4 zoomed grid with a spatial resolution of approximately 50 km by the IDW method. (5) The optimal trained model and bias correction methods were applied to all grid points within a region and all months within a season.

For the implementation of models, uncertainty of the datasets resulting from the model structures, parameters, training and testing strategies is not even discussed.

Re: In the original manuscript, the uncertainty was partly analyzed, but not comprehensive. The plotted +/- one standard deviation in Figs. 5-6 shows the dispersion degree of the evaluation metrics (CC and RMSE) for the simulated results of all bias correction and data fusion methods over 100 trials. The standard deviations of CC and RMSE calculated by LS and DT corrected simulations are smaller, while those calculated by BP, LSTM and CNN fused simulations are larger. The standard deviation of CC and RMSE calculated by the CNN fused simulations is the smallest among fusion methods. It can be considered that LS and DT correction methods show smaller uncertainties in CC and RMSE than the BP, LSTM and CNN fusion methods. CNN fusion methods show smaller uncertainties than the other two fusion methods.

In the revised manuscript, an uncertainty analysis for the use of data fusion methods was further analyzed. Specifically, the CNN method was taken as an example to analyze the uncertainty derived from model structure, model parameters and training samples for fusing isotope in South China (SC) over summer (JJA). For the model structure, a different number of convolution layers were selected, because the model is very sensitive to the number of convolution layers (Mboga et al., 2017). For model parameters, three parameters, namely learning rate, batch size and filter size, were selected based on previous sensitivity studies (Zhang and Wallace, 2015; Taylor et al., 2021; Mboga et al., 2017; Bengio, 2012). Commonly-used values for each parameter were selected to form twelve groups of parameter setting schemes. For the training sample, five different training-test sets were randomly generated. To sum up, the modelling combination scheme for uncertainty analysis is shown in Table 1.

A variance decomposition method (Song et al., 2020; Bosshard et al., 2013) was used to calculate the uncertainty contribution for these three sources as well as their interactions. The correlation coefficient (CC) and root mean square error (RMSE) were used as the evaluation criteria. Then, all the combination schemes were trained and the evaluation criteria were calculated, which was repeated 30 times for each combination. Results shows that the accuracy (i.e. standard error) of CC and RMSE are respectively 0.0025 and 0.0127‰. The relative contribution of each source to the total uncertainty is shown in Fig. 1. As can be seen, there is little difference in the relative contribution of uncertainty sources between the two evaluation criteria. Model parameters have the greatest contribution to the total uncertainty with the contribution being more than 50%, while the contribution of training samples is the least, which is less than 1%. These results indicate that the model is robust and not very dependent on training data.

Table 1. The modeling combination scheme of uncertainty calculation.

Model structure	Model parameters			Training samples
Number of convolutional layer	Learning rate	Batch size	Filter size	
1	0.0005	20	3	
2	0.001	50	4	Samples 1-5
3	0.002			

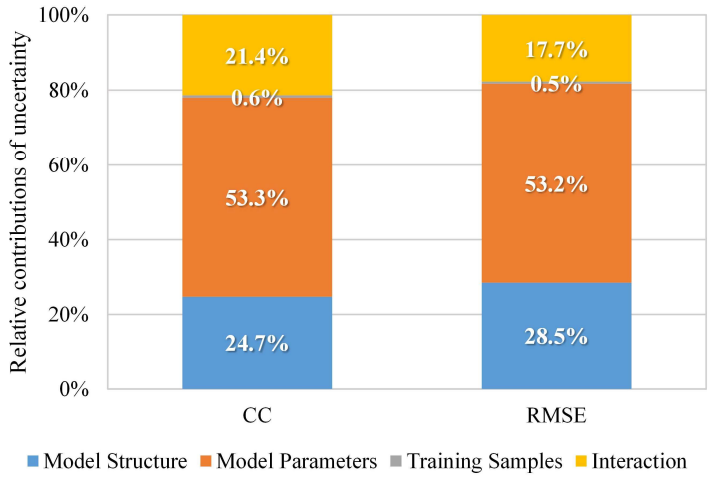

Figure 1. The relative contribution of each source to the total uncertainty.

References:

Bengio, Y.: Practical recommendations for gradient-based training of deep architectures, Neural networks: Tricks of the trade, Springer, Berlin, Heidelberg, 437-478, https://doi.org/10.1007/978-3-642-35289-8_26, 2012.

Bosshard, T., Carambia, M., Goergen, K., Kotlarski, S., Krahe, P., Zappa, M., and Schär, C.: Quantifying uncertainty sources in an ensemble of hydrological climate-impact projections, Water Resources Research, 49, 1523-1536, https://doi.org/10.1029/2011WR011533, 2013.

Mboga, N., Persello, C., Bergado, J. R., and Stein, A.: Detection of informal settlements from VHR images using convolutional neural networks, Remote sensing, 9, 1106, https://doi.org/10.3390/rs9111106, 2017.

Song, T., Ding, W., Liu, H., Wu, J., Zhou, H., and Chu, J.: Uncertainty quantification in machine learning modeling for multi-step time series forecasting: Example of recurrent neural networks in discharge simulations, Water, 12, 912, https://doi.org/10.3390/w12030912, 2020.

Taylor, R., Ojha, V., Martino, I., and Nicosia, G.: Sensitivity analysis for deep learning: ranking hyper-parameter influence, 2021 IEEE 33rd International Conference on Tools with Artificial Intelligence (ICTAI), 512-516, https://doi.org/10.1109/ICTAI52525.2021.00083, 2021.

Zhang, Y., and Wallace, B.: A sensitivity analysis of (and practitioners' guide to) convolutional neural networks for sentence classification, arXiv [preprint], arXiv:1510.03820, 2015.

Data-quality assessment at finer scale is poor presented. I have concerns about the reliability of spatial-temporal variations in your new data product at fine resolution.

Re: Thanks lot for the insightful comments. **Following the reviewer's comments, a comprehensive**

assessment of the dataset at the finer scale was conducted. Specifically, the dataset was evaluated with respect to reproducing the time-series of in-situ observations at station scale, as well as the spatial pattern for each month. The detailed procedures are presented as follows.

To evaluate the dataset for all stations, the correlation coefficient (CC) and root mean square error (RMSE) were calculated for $\delta^{18}O_p$ series between observations and raw iGCM simulations, and between observations and built isoscape for all stations over the common period (Tables 2-3). The results show that the built isoscape performs excellent for the vast majority of stations, with larger CCs and smaller RMSEs than iGCM simulations. Specifically, the CCs between the isoscape simulations and observations are larger than 0.8 for 73% of the stations and larger than 0.9 for 49% of the stations. The RMSEs between the isoscape simulations and observations are smaller than 20‰ for 78% of the stations and less than 15‰ for 56% of the stations.

To further demonstrate the dataset quality, two stations with appropriate length of observation were randomly selected for each sub-region. Totally, 12 stations were selected. The time series of $\delta^{18}O_p$ were plotted for observations, iGCM simulations, and the generated isoscape (Fig. 2). As can be seen from Fig. 2, the variations of $\delta^{18}O_p$ are very consistent between the generated isoscape and observations, and the isoscape performs much better than raw iGCM simulations. In particular for the period before 2007, the CNN model integrates the advantages of various simulations and captures most features of the observed data. These results generally prove that the generated isoscape is reliable.

Fig. 3 further shows the monthly spatial distribution of observed, newly generated, and better-performing simulated $\delta^{18}O_p$ for their common period (i.e. 1979-2007). The spatial pattern presented by the built isoscape shows the best consistency with the observations. The strength of the CNN model has been demonstrated, which can make good use of the advantages of each simulation to accurately capture the characteristics of observations. For example, the LMDZ nudged model shows a strong ability to reproduce the spatial distribution of $\delta^{18}O_p$ for the eastern region in summer and autumn, but a slightly poor performance in the Qinghai-Tibet Plateau. The built isoscape combines LMDZ nudged with GISS nudged and LMDZ zoomed simulations, which show reasonably performance for the Qinghai-Tibet Plateau, and well reproduces the spatial distribution of $\delta^{18}O_p$ for mainland China.

In addition, based on suggestions from other reviewers, we will introduce some physical-based ancillary data in the fusion, such as elevation and meteorological data. Taking into account the effects of elevation and meteorological factors on precipitation isotopes might make our dataset more reliable.

From above analyzes, we are very confident that the generated isoscape is of high quality and the best dataset available in China, which will be widely used in the future. All above results will be added in the revised manuscript.

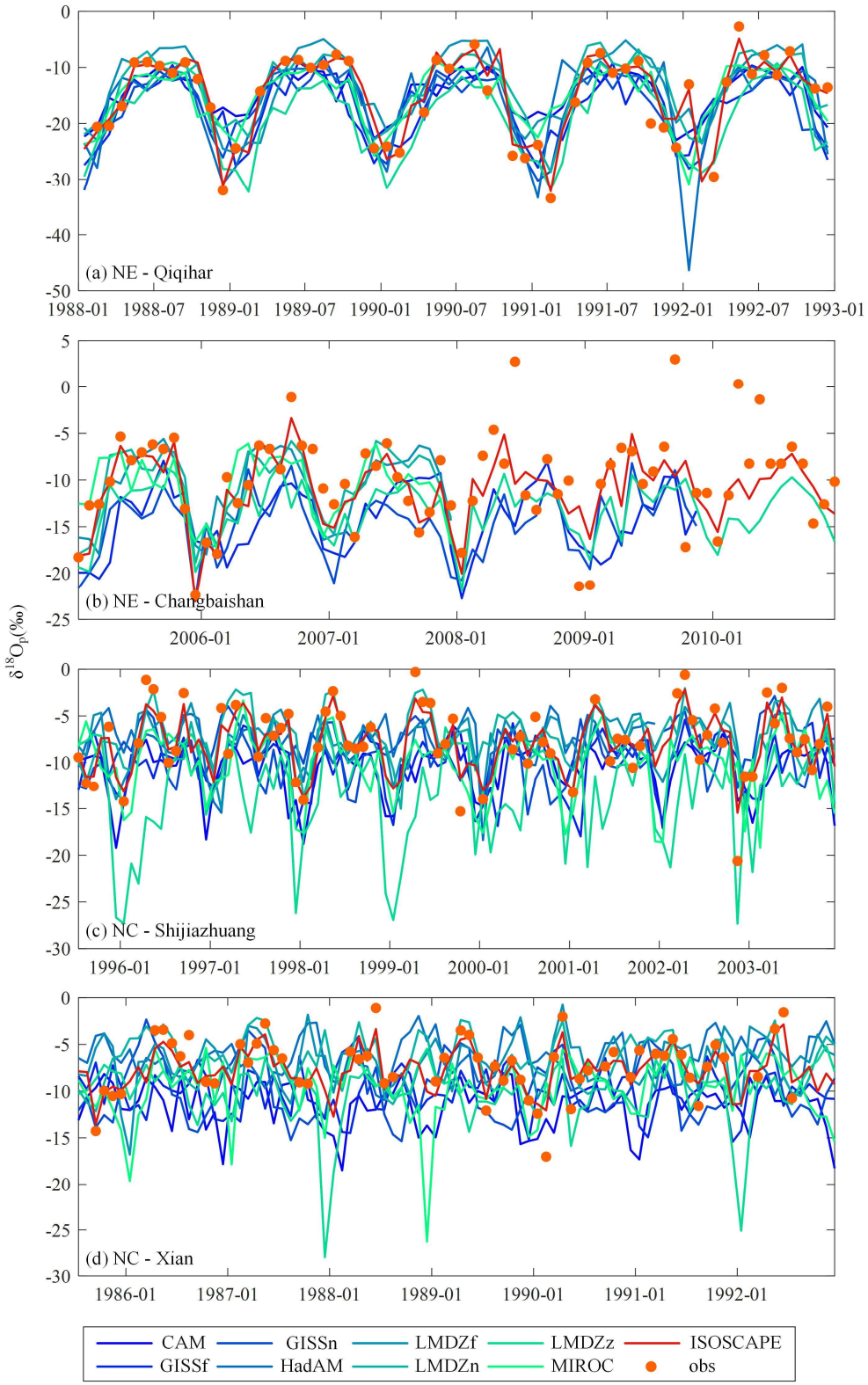

Figure 2. Time-series comparisons of $\delta^{18}O_p$ among the built isoscape, iGCM simulations, and in-situ observations at selected stations in each sub-region.

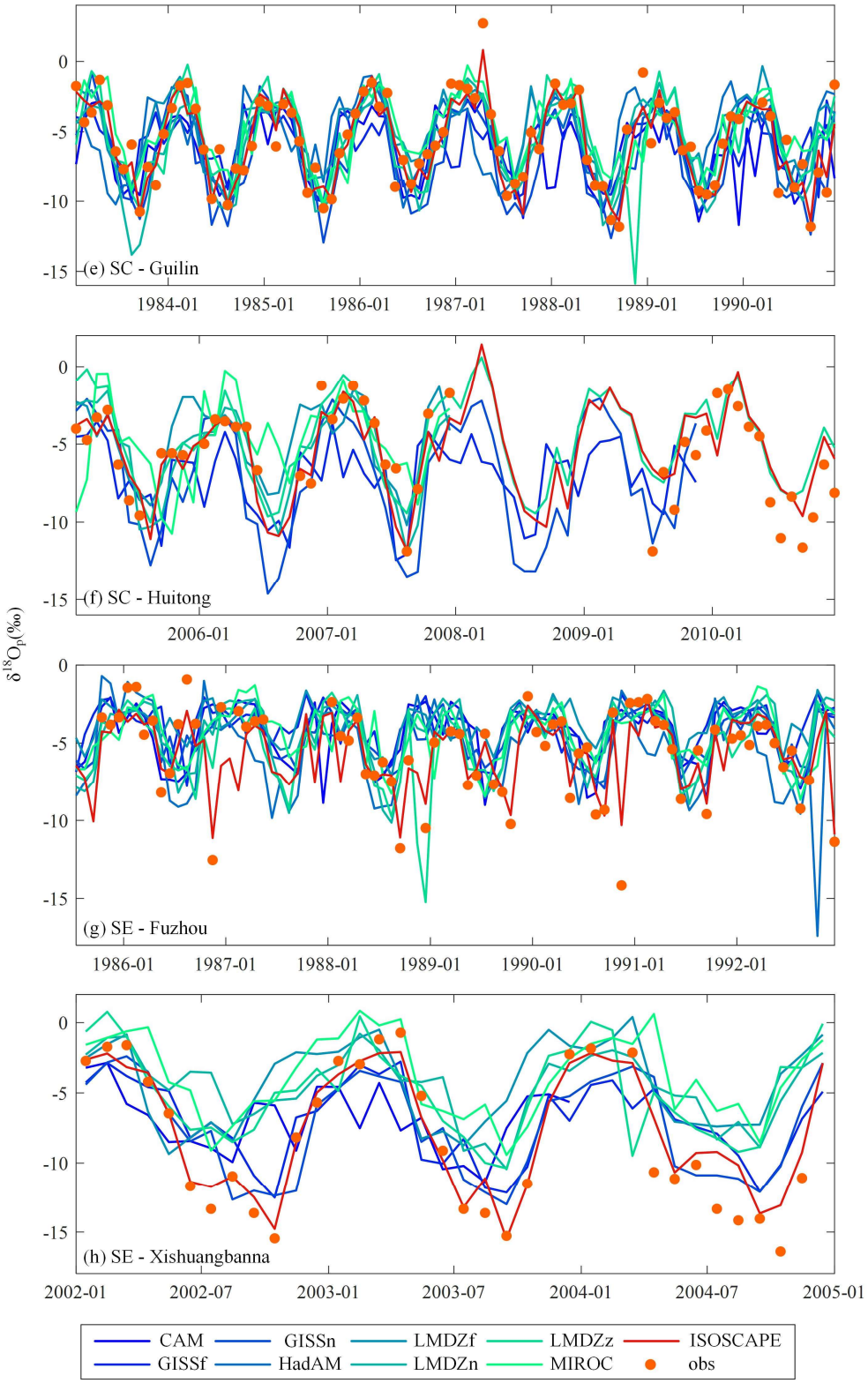

Figure 2. Time-series comparisons of $\delta^{18}O_p$ among the built isoscape, iGCM simulations, and in-situ observations at selected stations in each sub-region.

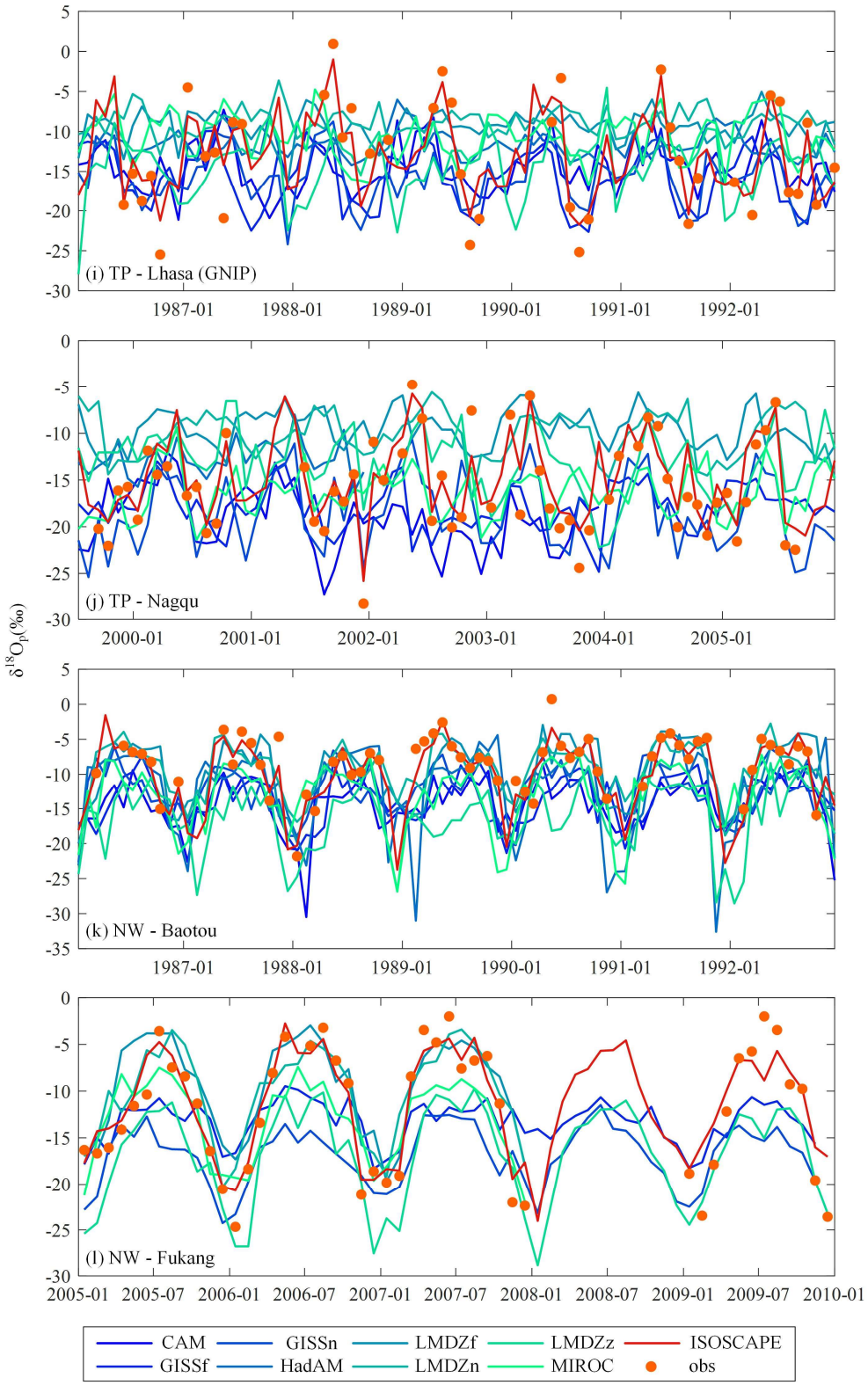

Figure 2. Time-series comparisons of $\delta^{18}O_p$ among the built isoscape, iGCM simulations, and in-situ observations at selected stations in each sub-region.

Table 2. Correlation coefficient (CC) metrics of $\delta^{18}O_p$ series between observations and iGCM simulations and the built isoscape at all stations.

Subregion	Station	Isoscape	CAM	GISSf	GISSn	HadAM	LMDZf	LMDZn	LMDZz	MIROC
NE	Changchun	0.93	0.80	0.74	0.77	0.64	0.68	0.86	0.63	0.68
NE	Haerbin	0.89	0.38	0.33	0.66	0.36	0.45	0.53	0.47	0.46
NE	Qiqihar	0.97	0.71	0.63	0.78	0.58	0.74	0.81	0.79	0.68
NE	Changbaishan	0.69	/	0.46	0.60	/	0.59	0.72	0.51	0.58
NE	Sanjiang	0.97	/	0.46	0.51	/	0.55	0.63	0.65	0.38
NE	Hailun	0.93	/	0.74	0.73	/	0.72	0.76	0.74	0.69
NE	Shenyang	0.28	/	0.02	0.13	/	-0.25	0.18	-0.09	0.05
NC	Jinzhou	0.82	-0.19	0.03	0.34	0.30	0.42	0.48	-0.46	0.25
NC	Shijiazhuang	0.95	0.33	0.28	0.33	0.22	0.31	0.55	0.27	0.32
NC	Taiyuan	0.98	0.17	0.27	-0.16	-0.38	-0.12	-0.09	-0.14	0.27
NC	Tianjin	0.95	0.43	0.51	0.29	0.41	0.43	0.66	0.12	0.40
NC	Xian	0.92	0.12	-0.02	0.41	-0.23	0.20	0.59	0.30	0.41
NC	Yantai	0.95	0.18	0.07	0.46	0.23	0.16	0.48	-0.27	0.23
NC	Zhengzhou	0.91	0.07	0.18	0.49	0.00	0.22	0.56	0.08	0.39
NC	Beijing	0.68	/	0.75	0.23	/	0.78	0.74	0.60	0.80
NC	Fengqiu	0.90	/	0.05	0.77	/	0.26	0.66	0.09	0.20
NC	Yucheng	0.72	/	0.28	0.30	/	0.25	0.54	0.08	0.47
NC	Changwu	0.90	/	-0.36	0.50	/	-0.02	0.69	0.10	0.07
SC	Changsha	0.91	0.45	0.50	0.69	0.16	0.56	0.76	0.62	0.53
SC	Chengdu	0.87	0.43	0.17	0.67	-0.05	0.39	0.68	0.66	0.52
SC	Guilin	0.94	0.59	0.55	0.86	0.43	0.71	0.79	0.79	0.71
SC	Guiyang	0.95	0.31	0.46	0.75	0.25	0.54	0.78	0.82	0.55
SC	Kunming	0.97	0.55	0.62	0.82	0.47	0.65	0.86	0.66	0.68
SC	Liuzhou	0.87	0.53	0.52	0.74	0.49	0.64	0.74	0.72	0.71
SC	Wuhan	0.92	0.37	0.25	0.64	0.09	0.36	0.70	0.64	0.51
SC	Zunyi	0.91	0.29	0.41	0.76	0.24	0.54	0.80	0.79	0.51
SC	Yingtan	0.63	/	0.07	0.35	/	0.31	0.22	0.42	0.18
SC	Taoyuan	0.83	/	0.53	0.82	/	0.56	0.76	0.78	0.40
SC	Qianyanzhou	0.87	/	0.12	0.59	/	0.40	0.63	0.59	0.54
SC	Huitong	0.81	/	0.45	0.77	/	0.69	0.80	0.78	0.45
SC	Yanting	0.71	/	0.32	0.43	/	/	/	0.72	/
SC	Heshang	0.77	/	/	/	/	/	/	0.73	/
SC	Changsha	0.82	/	/	/	/	/	/	0.79	/
SE	Fuzhou	0.89	0.24	0.09	0.50	0.24	0.23	0.37	0.52	0.33
SE	Guangzhou	0.90	0.36	0.60	0.60	0.47	0.61	0.58	0.44	0.44
SE	Hong Kong	0.80	0.61	0.60	0.79	0.64	0.68	0.78	0.64	0.62
SE	Nanjing	0.96	0.25	0.37	0.62	0.31	0.34	0.73	0.35	0.24
SE	Changshu	0.91	/	0.29	0.79	/	0.41	0.74	0.73	0.13
SE	Dinghushan	0.45	/	0.39	0.69	/	0.97	1.00	0.49	1.00
SE	Ailaoshan	0.97	/	0.66	0.87	/	0.70	0.83	0.14	0.80
SE	Guangzhou	0.74	/	0.47	0.84	/	0.91	0.83	0.64	0.77
SE	Yongan	0.43	/	/	/	/	/	/	0.35	/
SE	Xishuangbanna	0.96	0.53	0.82	0.85	/	0.57	0.78	0.68	0.78
SE	Guangzhou	0.77	/	0.51	0.83	/	0.79	0.76	0.73	0.64
TP	Lhasa	0.94	0.19	0.39	0.59	0.37	0.13	0.13	0.19	0.20

Subregion	Station	Isoscape	CAM	GISSf	GISSn	HadAM	LMDZf	LMDZn	LMDZz	MIROC
TP	Lhasa	0.78	/	0.58	0.59	/	0.36	0.19	0.27	0.45
TP	Haibei	0.87	/	0.24	0.30	/	0.64	0.50	0.43	0.40
TP	Maoxian	0.58	/	-0.39	0.48	/	0.07	0.66	0.45	0.13
TP	Gonggashan	0.71	/	0.10	0.68	/	0.32	0.62	0.69	0.36
TP	Delingha	0.98	0.27	0.45	0.75	0.75	0.80	0.85	0.80	0.73
TP	Nagqu	0.92	0.17	0.16	0.64	0.15	0.15	0.06	0.46	0.40
TP	Yushu	0.81	0.00	-0.12	0.37	-0.11	0.18	0.28	0.46	0.29
TP	Gaize	0.96	0.34	0.03	0.44	-0.06	0.36	0.37	0.43	0.18
TP	Shiquanhe	0.79	-0.33	0.25	0.35	-0.06	0.46	0.35	0.43	0.04
TP	Lhasa	0.94	0.37	0.63	0.74	0.45	0.45	0.40	0.42	0.56
TP	Dingri	0.89	-0.08	0.61	0.18	0.71	-0.33	0.44	0.37	0.35
TP	Nyalam	0.92	0.40	0.46	0.69	-0.06	0.48	0.32	0.35	0.48
TP	Tuotuohe	0.94	0.18	0.10	0.64	0.44	0.66	0.67	0.67	0.48
TP	Baidi	0.84	/	0.51	0.62	/	0.29	0.47	0.44	0.49
TP	Dui	0.87	/	0.56	0.53	/	0.34	0.28	0.39	0.43
TP	Taxkorgen	0.97	0.19	0.70	0.79	/	0.80	0.82	0.83	0.70
TP	Wengguo	0.87	/	0.66	0.57	/	0.29	0.53	0.63	0.56
TP	Lulang	0.80	/	0.45	0.76	/	0.63	0.62	0.68	0.27
TP	Nuxia	0.59	/	-0.21	0.79	/	/	/	0.49	/
TP	Yeniugou	0.84	/	0.88	0.83	/	/	/	0.88	/
NW	Baotou	0.93	0.43	0.52	0.51	0.39	0.43	0.60	0.28	0.46
NW	Hetian	0.96	0.49	0.52	0.82	0.55	0.81	0.89	0.88	0.82
NW	Lanzhou	0.94	0.18	0.22	-0.07	0.53	0.60	0.60	0.45	0.61
NW	Wulumuqi	0.97	0.40	0.67	0.76	0.76	0.78	0.86	0.87	0.73
NW	Yinchuan	0.95	0.43	0.58	0.34	0.45	0.62	0.76	0.75	0.63
NW	Zhangye	0.96	0.35	0.59	0.57	0.62	0.80	0.83	0.79	0.76
NW	Fukang	0.94	/	0.75	0.78	/	0.87	0.88	0.86	0.84
NW	Cele	0.90	/	-0.38	0.66	/	0.59	0.79	0.72	0.55
NW	Linze	0.93	/	0.68	0.67	/	0.78	0.79	0.68	0.81
NW	Shapotou	0.48	/	0.14	0.20	/	0.30	0.30	-0.10	0.17
NW	Ansai	0.73	/	-0.06	0.53	/	-0.04	0.66	0.00	0.33
NW	Erdos	0.19	/	0.01	0.70	/	0.33	0.13	0.17	-0.54
NW	Naiman	0.88	/	0.62	0.64	/	0.55	0.42	0.75	0.11

Table 3. Root mean square error (RMSE, ‰) metrics of $\delta^{18}O_p$ series between observations and iGCM simulations and the built isoscape at all stations.

Subregion	Station	Isoscape	CAM	GISSf	GISSn	HadAM	LMDZf	LMDZn	LMDZz	MIROC
NE	Changchun	7.47	11.50	14.71	14.98	17.35	16.14	11.45	22.16	13.80
NE	Haerbin	8.31	20.78	24.55	31.03	22.20	20.36	16.32	23.95	20.69
NE	Qiqihar	13.67	38.19	43.10	34.59	50.34	39.30	33.69	38.38	38.57
NE	Changbaishan	31.87	/	47.09	46.38	/	22.75	18.46	45.71	21.93
NE	Sanjiang	9.31	/	34.13	33.77	/	31.78	24.98	24.61	29.68
NE	Hailun	16.44	/	26.52	32.42	/	27.26	26.73	26.57	26.28
NE	Shenyang	20.70	/	24.61	20.10	/	22.11	12.67	33.25	17.39
NC	Jinzhou	5.46	10.88	8.25	6.59	7.97	6.56	6.68	21.52	11.30
NC	Shijiazhuang	15.12	56.29	49.40	45.68	40.41	44.44	36.17	83.95	52.45
NC	Taiyuan	5.37	22.94	23.43	24.56	20.93	19.33	20.78	33.76	19.09
NC	Tianjin	9.34	31.11	25.51	24.90	25.79	24.63	18.78	54.64	31.35
NC	Xian	10.27	40.99	35.42	32.86	32.12	28.35	20.92	30.46	26.61
NC	Yantai	5.84	19.21	21.43	18.19	18.76	20.83	17.23	36.96	24.88
NC	Zhengzhou	10.99	36.21	32.11	23.59	26.80	25.12	20.52	42.04	23.46
NC	Beijing	28.37	/	20.28	27.08	/	14.61	14.19	29.14	10.71
NC	Fengqiu	10.03	/	22.74	17.20	/	18.24	14.66	27.88	19.44
NC	Yucheng	13.78	/	21.10	19.83	/	17.29	15.57	31.43	15.38
NC	Changwu	13.79	/	40.64	37.52	/	21.68	13.69	31.02	28.30
SC	Changsha	9.74	21.83	23.99	22.08	27.34	19.65	15.59	19.36	19.72
SC	Chengdu	16.55	56.26	56.99	62.06	39.34	29.57	25.76	26.21	43.54
SC	Guilin	10.18	24.79	24.69	19.40	29.09	21.52	19.23	18.46	21.60
SC	Guiyang	9.14	31.95	26.87	23.28	30.90	25.78	19.23	22.24	25.05
SC	Kunming	16.06	47.73	44.50	44.59	44.75	47.67	40.91	47.68	45.03
SC	Liuzhou	11.06	20.81	19.86	16.67	21.12	18.23	16.09	17.71	16.44
SC	Wuhan	7.79	19.69	24.96	19.37	24.38	20.34	15.64	16.61	17.62
SC	Zunyi	13.82	38.47	33.45	31.05	34.47	28.45	21.06	22.14	28.87
SC	Yingtan	17.72	/	22.76	25.17	/	13.90	19.02	22.05	14.57
SC	Taoyuan	11.19	/	17.54	15.16	/	13.78	11.46	14.23	16.38
SC	Qianyanzhou	7.51	/	20.86	18.09	/	14.37	13.41	13.93	13.33
SC	Huitong	12.06	/	18.17	15.19	/	10.52	9.30	14.60	15.35
SC	Yanting	21.13	/	31.54	33.49	/	/	/	20.09	/
SC	Heshang	20.75	/	/	/	/	/	/	21.97	/
SC	Changsha	19.15	/	/	/	/	/	/	21.62	/
SE	Fuzhou	10.88	27.18	28.32	22.42	27.09	28.15	25.79	21.75	25.71
SE	Guangzhou	6.39	15.12	10.76	10.91	16.41	11.04	13.11	17.21	13.25
SE	Hong Kong	38.15	43.96	47.98	34.52	50.52	42.01	32.63	45.53	40.70
SE	Nanjing	6.91	22.14	19.21	17.01	23.01	25.58	20.30	22.12	24.79
SE	Changshu	3.50	/	9.88	5.73	/	14.49	10.67	6.84	11.59
SE	Dinghushan	22.85	/	15.51	14.40	/	3.71	1.20	22.44	5.39
SE	Ailaoshan	6.46	/	20.21	15.92	/	27.27	24.72	33.50	25.93
SE	Guangzhou	20.37	/	16.56	9.74	/	5.71	6.20	23.52	6.89
SE	Yongan	15.83	/	/	/	/	/	/	16.42	/
SE	Xishuangbanna	9.26	20.69	19.55	16.55	/	32.37	29.43	28.11	32.21
SE	Guangzhou	11.43	/	16.95	11.17	/	9.01	8.77	12.06	9.43
TP	Lhasa	16.48	45.39	48.24	40.56	42.23	50.30	53.37	43.84	46.20

Subregion	Station	Isoscape	CAM	GISSf	GISSn	HadAM	LMDZf	LMDZn	LMDZz	MIROC
TP	Lhasa	24.27	/	30.61	30.51	/	34.27	37.35	36.78	30.10
TP	Haibei	11.23	/	38.38	45.39	/	21.11	19.96	33.95	29.98
TP	Maoxian	13.61	/	25.84	29.51	/	13.38	9.50	15.67	12.89
TP	Gonggashan	27.37	/	26.75	31.77	/	26.49	24.21	30.24	23.97
TP	Delingha	14.94	87.68	127.83	113.21	53.20	40.92	35.78	85.71	71.41
TP	Nagqu	16.24	40.61	42.90	35.18	25.44	61.90	62.31	40.53	35.25
TP	Yushu	11.73	32.84	50.28	37.89	13.08	31.88	29.51	20.69	29.43
TP	Gaize	13.95	44.70	72.06	53.95	31.61	51.14	50.41	40.32	47.10
TP	Shiquanhe	20.98	37.84	33.23	32.83	30.81	50.83	49.15	35.91	51.55
TP	Lhasa	22.86	48.17	51.15	47.12	41.72	75.87	79.16	57.43	61.10
TP	Dingri	9.82	20.02	17.23	25.29	13.54	41.22	40.39	20.09	39.40
TP	Nyalam	22.22	44.29	48.22	37.36	65.87	56.07	58.01	52.53	64.70
TP	Tuotuohe	22.46	84.32	112.41	78.12	48.50	56.33	55.78	45.39	60.21
TP	Baidi	12.24	/	21.66	20.40	/	33.47	32.83	23.63	36.25
TP	Dui	17.57	/	28.75	28.00	/	43.04	43.72	34.06	44.76
TP	Taxkorgen	12.64	13.27	44.91	48.34	/	31.72	30.37	32.65	34.84
TP	Wengguo	10.97	/	15.37	17.58	/	29.67	29.66	19.67	31.43
TP	Lulang	39.66	/	29.51	25.03	/	27.43	26.70	44.52	22.53
TP	Nuxia	25.64	/	10.31	14.28	/	/	/	24.23	/
TP	Yeniugou	16.60	/	30.61	37.42	/	/	/	16.30	/
NW	Baotou	11.33	50.59	42.77	38.48	43.78	32.82	24.41	60.87	40.64
NW	Hetian	19.61	60.60	67.10	77.90	76.83	36.28	31.10	61.56	38.01
NW	Lanzhou	10.60	55.48	53.01	65.13	28.74	24.34	23.92	38.27	42.90
NW	Wulumuqi	17.15	66.80	59.34	69.90	63.51	55.43	44.56	69.41	49.72
NW	Yinchuan	8.14	38.30	33.31	35.84	27.23	21.02	18.36	33.55	29.89
NW	Zhangye	20.80	84.71	91.43	93.86	53.70	40.24	37.27	65.15	64.30
NW	Fukang	17.91	/	35.66	46.33	/	23.33	21.36	40.93	23.37
NW	Cele	8.46	/	49.74	52.79	/	18.44	17.65	32.59	25.31
NW	Linze	16.52	/	48.37	51.71	/	21.65	21.60	47.16	30.30
NW	Shapotou	18.98	/	41.20	52.35	/	14.44	16.28	41.61	23.84
NW	Ansai	18.09	/	38.55	32.02	/	24.17	13.92	37.28	23.82
NW	Erdos	14.76	/	22.65	20.64	/	7.69	9.35	24.33	11.91
NW	Naiman	12.76	/	13.85	13.75	/	12.61	12.42	36.06	14.49

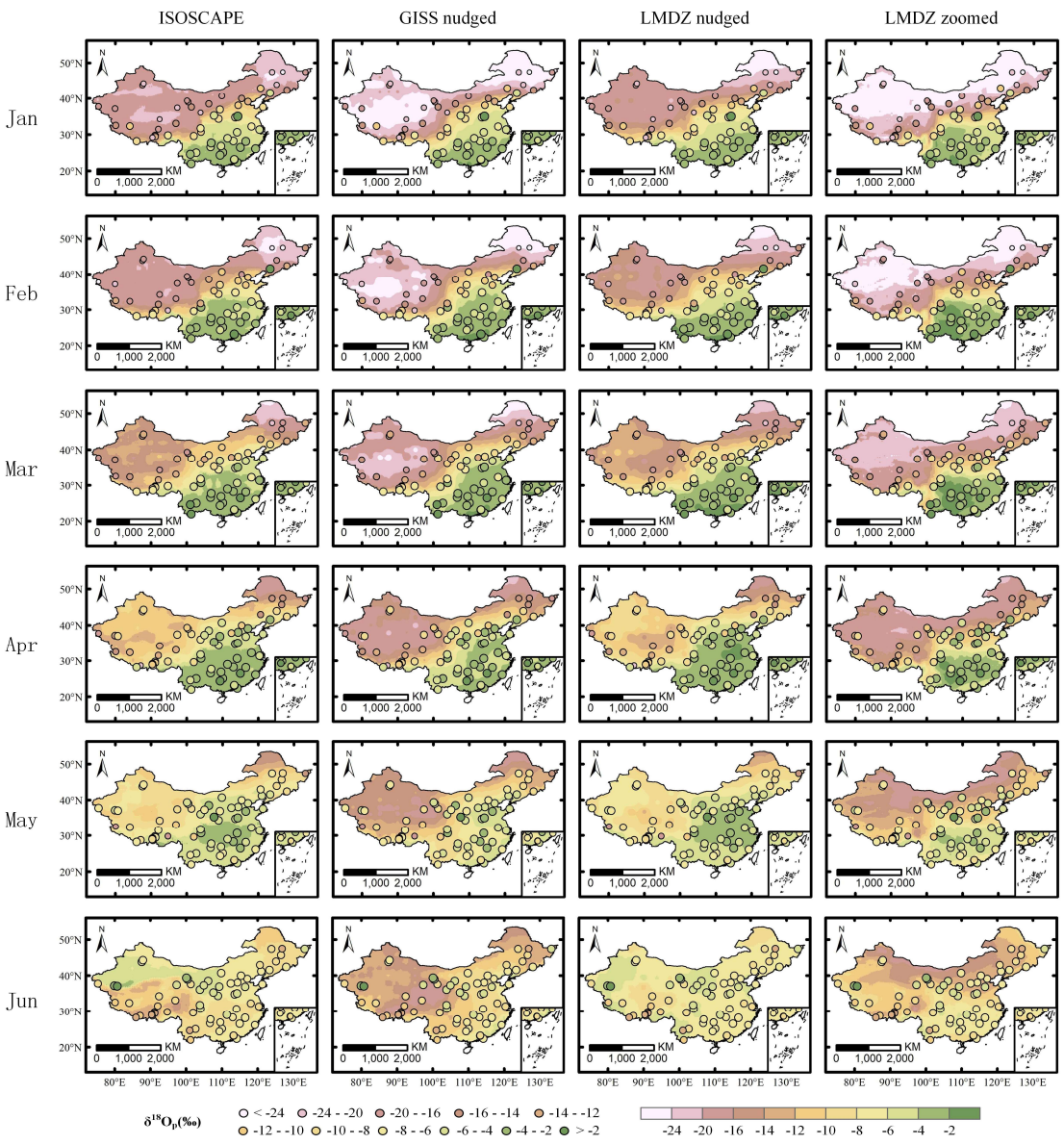

Figure 3. Spatial distributions of $\delta^{18}O_p$ in each month for the period of 1979-2007 as obtained from observations (circles), the built isoscape (left column), and better-performing iGCMs (right three columns).

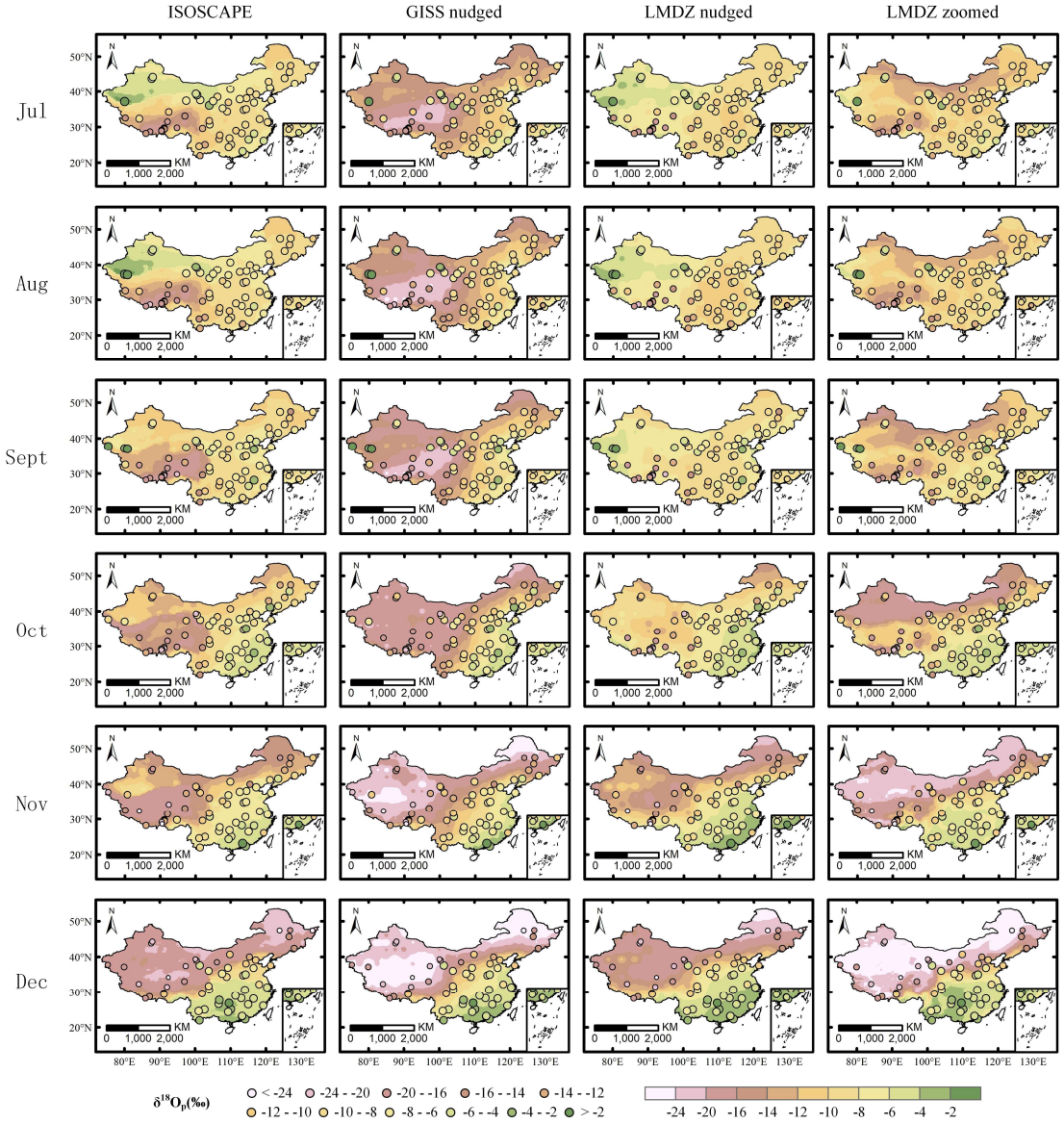

Figure 3. Spatial distributions of $\delta^{18}O_p$ in each month for the period of 1979-2007 as obtained from observations (circles), the built isoscape (left column), and better-performing iGCMs (right three columns).